Department of Mathematics and Statistics
College of Engineering

UC
UNIVERSITY OF CANTERBURY
Te Whare Wānanga o Waitaha
CHRISTCHURCH NEW ZEALAND

Summer Research Project

Lagrangian Coherent Structures

By Matthew Botur

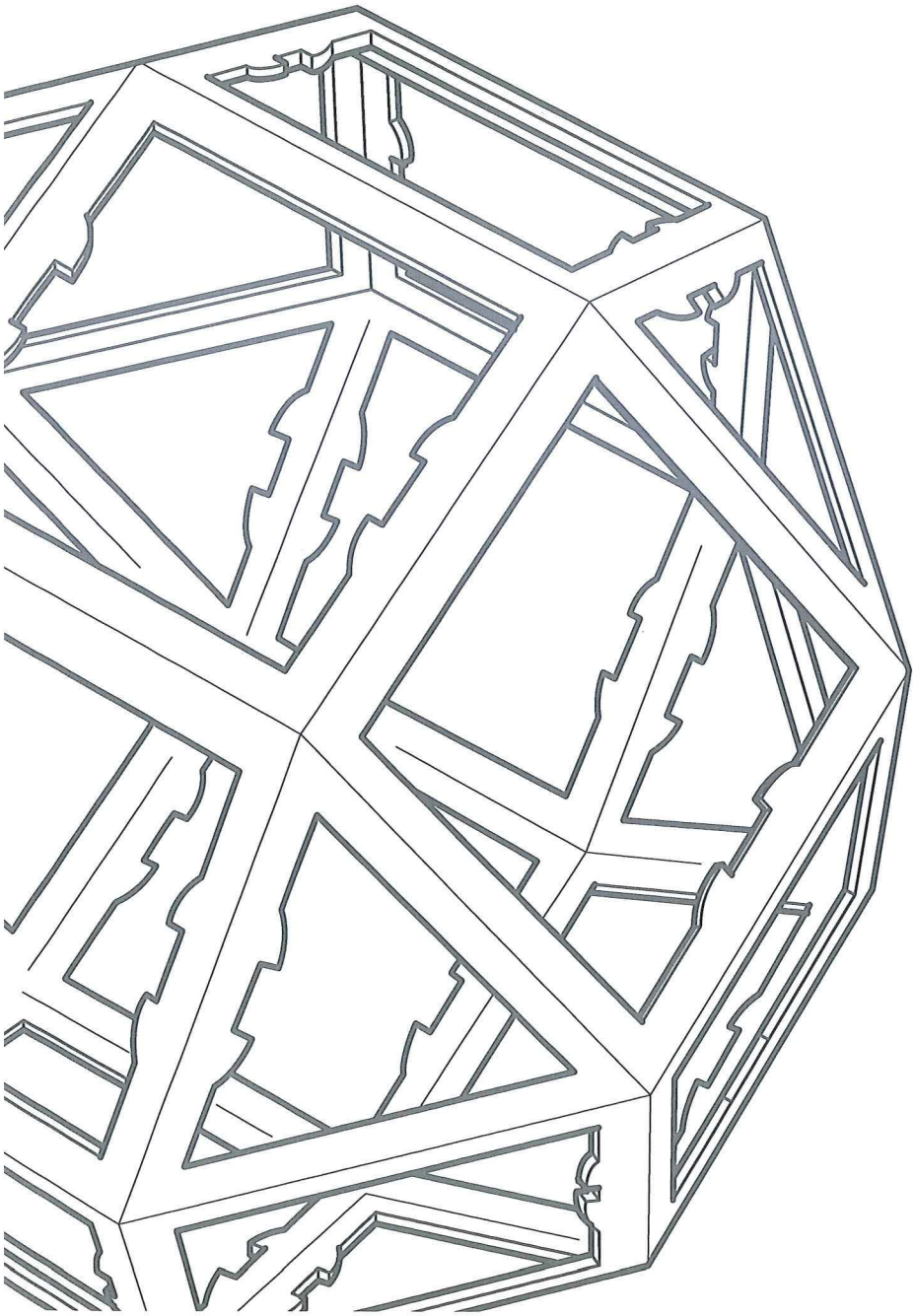

09

Lagrangian Coherent Structures

Matthew Botur

February 4, 2009

Though dynamical systems are a popular area of research these days, previous methods have dealt poorly with non-autonomous systems. Invariant manifolds are not easily found if they too are advected by the flow. Lagrangian methods, however, can deal with such behaviour, looking at the finite-time Lyapunov exponent (FTLE) of each point in the field as a behavioural guide. This paper seeks to understand the nature of these FTLE fields, and the Lagrangian Coherent Structures (LCSs) they contain. To this end, precise definitions are developed and explored, allowing the construction of algorithms for the computation of the FTLE field, as well as the extraction of the LCS.

Introduction

Traditional dynamical system analysis involves a Eulerian approach, where properties are considered according to a single, fixed frame of reference. For systems without time dependence (i.e. autonomous systems), as well as those that are strongly periodic, such an approach is important towards understanding the behaviour of the system over time. However, many, if not most, real world systems do exhibit time dependence (i.e. non-autonomous systems), and as such traditional perspectives are of less use. Especially where studying transport flows, a Lagrangian approach is of more use. Here changes are considered as they occur to a particle, which is followed along a trajectory.

Even for velocity fields of relatively simple form, individual trajectories may be surprisingly complex. Such a phenomenon is referred to as deterministic chaos, or chaotic transport, and is generally non-evident from inspection of system equations. For time-independent and time periodic flows, the invariant manifolds of fixed points and periodic orbits divide the system into mixing templates, distinct regions of the flow exhibiting qualitatively different dynamics. These greatly simplify the task of system analysis, providing useful qualitative and quantitative information with a minimum of computational effort.

When the system has general time dependence, however, determination of such invariant sets is usually not available, at least not in their usual meaning. Instead we look to emergent patterns of the flow known as *coherent structures*, which have similar properties to invariant

sets. When coherent structures are studied in terms of quantities derived from fluid trajectories, they are considered Lagrangian Coherent Structures (LCS). How these structures are detected is an important question, especially as they are often only vaguely defined. Over a series of papers, Haller et al (2000, 2000, 2000, 2001) attempted to give a more precise definition of LCSs for general time-dependent systems, defined over a finite time interval. Two alternative definitions were given; his first was based on invariants of the gradient of the velocity field evaluated along fluid trajectories. In this manner, LCSs were defined by local extrema of the hyperbolic time field, which measures how long each trajectory remains hyperbolic. The second definition, which we base our study around, gives the LCS as local extrema of the finite-time Lyapunov exponent (FTLE) field. It should also be noted that Haller (2001) shows a strong correspondence between LCSs computed in each manner for steady and forced Arnold-Beltrami-Childress flows.

The Lyapunov exponent (or Lyapunov characteristic exponent) is a quantity that characterizes the asymptotic rate of separation of infinitesimally close trajectories. Much literature details their use, such as Liapunov (1966) and Barreira and Pesin (2002). More recently, Doerner et al. (1999) discussed how level contours of *finite-time* Lyapunov exponent fields can approximate stable manifolds for time-independent and periodic systems, and Pierrehumbert and Yang (1993) used FTLE fields to capture chaotic mixing regions and transport barriers from atmospheric data. This paper follows Shadden et al. (2005) in their formalization of the LCS as a ridge of the FTLE field, an approach first introduced by Haller (2002). Furthermore, most of the proofs in this work are heavily indebted to Shadden et al. (2005), whose superb paper on the subject was of great help in the completion of this study.

Our approach here is as follows. Section 1 introduces a few basic properties of the flow map, particularly useful for those new to dynamical systems. Section 2 then explains how the FTLE is calculated, following Shadden's approach. Restrictions are also placed on the systems to which we apply FTLE theory, limiting the scope of this paper appropriately. The FTLE definition is then used in Section 3, constructing a rigorous definition for the LCS. We compare and contrast two alternative definitions, which differ in their measures of curvature. Section 4 then looks at the issue of the Lagrangian nature of such structures. Ideally a LCS should be a material line advected by the flow, but are instead shown to be only *approximately* Lagrangian, evidencing a small material flux. The flux equation we derive then allows us to develop a set of conditions for an ideal LCS. Section 5 deals with the building of numerical algorithms for the computation of the FTLE fields, and the subsequent extraction of the LCS from these. Lastly, Section 6 then takes a brief look at a few applications of LCSs, in studying systems with arbitrary time dependence.

1. Notation and Definitions

Before we move towards defining the FTLE field, some basic properties of the system demand attention. In this paper we restrict our study to the domain $D \subset \mathbb{R}^2$, though similar study is possible in higher dimensional space. Given a time-dependent velocity field $\mathbf{v}(\mathbf{x}, t)$ defined on D, we define a trajectory $\mathbf{x}(t; t_0, \mathbf{x}_0)$ starting at point $\mathbf{x}_0 \in D$ at time t_0 to be the solution of

$$\begin{cases} \dot{\mathbf{x}}(t; t_0, \mathbf{x}_0) &= \mathbf{v}(\mathbf{x}(t; t_0, \mathbf{x}_0), t), \\ \mathbf{x}(t_0; t_0, \mathbf{x}_0) &= \mathbf{x}_0 \end{cases} \tag{1}$$

where $\dot{\mathbf{x}}$ is the derivative of $\mathbf{x}$ with respect to time.

Explicit here is that a trajectory is a function of time, but is also dependent on its initial conditions, both position $\mathbf{x}_0$ and time t_0. In keeping with these dependencies, and traditional fluid mechanics (Ottino (1989), Truesdell (1954)), we require the following assumption be made:

$$\textbf{A1.} \quad \textit{The velocity field } \mathbf{v}(x,t) \textit{ is at least } C^0 \textit{ in time and } C^3 \textit{ in space} \tag{2}$$

Consequently, $\mathbf{x}(t; t_0, \mathbf{x}_0)$ is C^1 in time and C^3 in space.

A solution of such a system is a map which takes points from an initial position $\mathbf{x}_0$ at time t_0 to their position at time t. We call this map a flow map, denoted by $\phi_{t_0}^t$, and satisfies

$$\phi_{t_0}^t : D \to D : \mathbf{x}_0 \mapsto \phi_{t_0}^t(\mathbf{x}_0) = \mathbf{x}(t; t_0, \mathbf{x}_0) \tag{3}$$

It follows from standard theorems on local existence and uniqueness of solutions of (1) that the map $\phi_{t_0}^t$ satisfies the following properties:

$$\begin{cases} \phi_{t_0}^{t_0}(\mathbf{x}) &= \mathbf{x}, \\ \phi_{t_0}^{t+s}(\mathbf{x}) &= \phi_s^{t+s}(\phi_{t_0}^s(\mathbf{x})) = \phi_t^{t+s}(\phi_{t_0}^t(\mathbf{x})) \end{cases} \tag{4}$$

and thus satisfies the properties of a semi-group.

2. The Finite Time Lyapunov Exponent

As stated previously, the Lyapunov exponent characterizes the asymptotic rate of separation of infinitesimally close trajectories. The FTLE is a finite-time average of the *maximum* rate of separation of two infinitesimally close trajectories. Consider two points, $\mathbf{x}$ and $\mathbf{y}$, where $\mathbf{y} = \mathbf{x} + \delta\mathbf{x}_0$ and $\delta\mathbf{x}_0$ is tiny (see figure 1). After advected by the flow for a time T, the separation between $\mathbf{x}$ and $\mathbf{y}$ is

$$\delta \mathbf{x}(T) = \phi_{t_0}^{t_0+T}(\mathbf{y}) - \phi_{t_0}^{t_0+T}(\mathbf{x}) = \frac{d\phi_{t_0}^{t_0+T}(\mathbf{x})}{d\mathbf{x}} \delta \mathbf{x}(0) + O(\| \delta \mathbf{x}(0) \|^2) \tag{5}$$

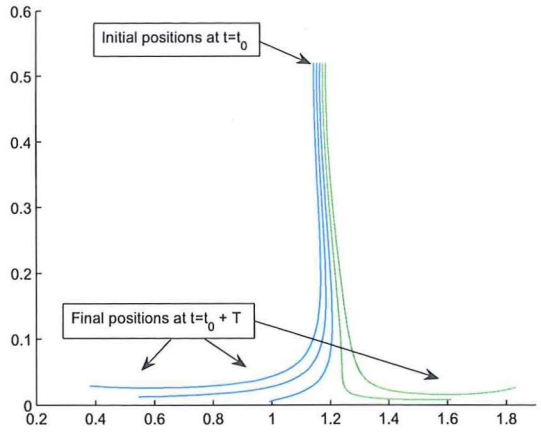

Figure 1: Trajectories on either side of a ridgeline separate over time

Where O is Landau notation for higher order terms small enough to ignore. By this formulation, we find the size of the perturbation as

$$\| \delta \mathbf{x}(T) \| = \sqrt{\left\langle \delta \mathbf{x}(0), \frac{d\phi_{t_0}^{t_0+T}(\mathbf{x})}{d\mathbf{x}}^* \frac{d\phi_{t_0}^{t_0+T}(\mathbf{x})}{d\mathbf{x}} \delta \mathbf{x}(0) \right\rangle} \tag{6}$$

where A^* denotes matrix multiplication by the transpose of A. From this definition we extract the (symmetric) matrix,

$$\triangle = \frac{d\phi_{t_0}^{t_0+T}(\mathbf{x})}{d\mathbf{x}}^* \frac{d\phi_{t_0}^{t_0+T}(\mathbf{x})}{d\mathbf{x}} \tag{7}$$

which is the finite-time version of the right Cauchy-Green deformation tensor. This tensor tells us how $\mathbf{x}$ 'stretches' in each direction when advected by the flow. Note that while we simply write $\triangle$, this is to avoid notational clutter; $\triangle$ also a function of $\mathbf{x}$, t_0 and T. It should be obvious that maximal stretching occurs when $\delta \mathbf{x}(0)$ is chosen to lie in the direction of the eigenvector associated with the maximum eigenvalue of $\triangle$. If we let $\overline{\delta \mathbf{x}}(0)$ take this alignment, then we can recast our expression for $\| \delta \mathbf{x}(T) \|$ as

$$\max_{\delta \mathbf{x}(0)} \| \delta \mathbf{x}(T) \| = \sqrt{\lambda_{\max}(\triangle)} \, \| \overline{\delta \mathbf{x}}(0) \| \tag{8}$$

This we then write as

$$\max_{\delta \mathbf{x}(0)} \parallel \delta \mathbf{x}(T) \parallel = e^{\sigma_{t_0}^{t_0+T}(\mathbf{x})|T|} \parallel \overline{\delta \mathbf{x}}(0) \parallel \tag{9}$$

where the FTLE, σ, is defined as

$$\sigma_{t_0}^{t_0+T}(\mathbf{x}) = \frac{1}{|T|} \ln \sqrt{\lambda_{\max}(\triangle)} \tag{10}$$

Notice that we have used $|T|$, not T, so as to permit backward-time integration. Negative T values enable the use of FTLEs for detecting *attracting* LCSs (analogous to unstable manifolds for autonomous systems), where positive T values enable detection of *repelling* LCSs (analogous to stable manifolds for autonomous systems). In fact, since $\frac{1}{|T|}$ is a scaling factor applied to the entire field, it may be dropped entirely during computation, without affecting the structures we hope to find. Figure 2 demonstrates a FTLE field computed in this manner, calculated for a periodically varying double-gyre. This is the system we shall use throughout this paper for our examples; see Appendix 1 for further details. We shall return to this point later when numerical methods are described, while using the unscaled version throughout the rest of this paper.

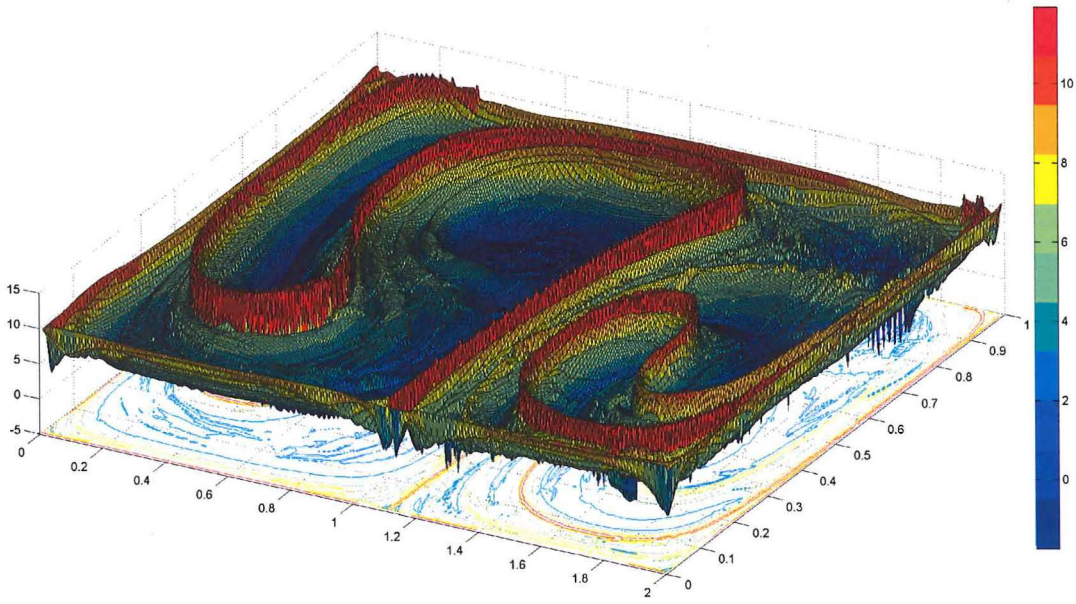

Figure 2: 3d FTLE field plot for non-autonomous double-gyre equation, t=0, T=15, 512x256 points

As a final simplification, we observe that since the spectral or L_2 norm is defined as $\parallel A \parallel_2 = \sqrt{\lambda_{\max}(A^*A)}$, where * is as before, σ can be rewritten more simply as

$$\sigma(\mathbf{x}) = \frac{1}{|T|} \ln \left\| \frac{d\phi_{t_0}^{t_0+T}(\mathbf{x})}{d\mathbf{x}} \right\|_2 \tag{11}$$

Once more we have dropped the explicit dependence on t_0 and T, to ease notational clutter. Equation (11) gives the *largest* finite-time Lyapunov exponent, where integrating over a finite time T at a fixed point $\mathbf{x}$ at time t_0. It is this FTLE which tells us how two extremely close points separate when advected by a flow; a large value implies a large degree of separation, a small value a small degree of separation. Ordinarily it would be expected that two extremely close points would move approximately together, only gradually separating over time. Therefore lines of high FTLE values give separatrices, or manifolds, where particles on either side follow very different trajectories, effectively separating the system into distinct mixing regions. It is important to understand that while an FTLE is computed at a point, it measures separation of neighbouring particles, and is consequently related to the grid spacing used. More on this point in section 5.

Before we move on to defining the LCS, we must take care to obey certain restrictions. Early work on Lyapunov exponents, such as by Oseledec (1989), requires us to limit this study to flows satisfying the exponential stretching hypothesis,

A2. *There is a constant k such that for all t*

$$\left\| \frac{d\phi_{t_0}^{t}(\mathbf{x})}{d\mathbf{x}} \right\| \leq e^{k|t-t_0|} \tag{12}$$

Such a restriction is due to the definition of Lyapunov exponents, which characterizes separation as $t \to \infty$. **A2** comes as a consequence of dealing with the *finite-time* Lyapunov exponent instead.

Furthermore, we are here only concerned with (finite-time) hyperbolic trajectories. These are trajectories where neighbouring particles compress in one direction and expand in another. More formally, this gives the assumption

$$\textbf{A3.} \quad \ln\, \lambda_{\min}(\triangle) < 0 < \ln\, \lambda_{\max}(\triangle) \tag{13}$$

Such a restriction is important, as it allows us to ignore areas of expansion or compression (i.e. sources and sinks). These correspond to situations where the logarithms of each eigenvalue of the Cauchy-Green deformation tensor have the same sign. We do not wish to look at these,

as such regions have no separating Lagrangian structure, and are as such less interesting, as well as less useful. Such a restriction also precludes lines of pure shear, which can otherwise be hard to distinguish from hyperbolic lines. Shear lines are those where points along the line remain fixed, while those off the line are shifted parallel to the line, by a distance proportional to their perpendicular distance from the line. Finally, an important consequence of equation (13) is that it guarantees that the two eigenvalues of $\triangle$ are distinct. Also, since $\triangle$ is a real and symmetric matrix, we know that both eigenvalues must be real and positive,. We then deduce that since $\phi_{t_0}^{t_0+T}(\mathbf{x})$ is C^3 in space and C^1 in time, $\triangle$ must be C^2 in space and C^1 in time. Therefore both eigenvalues are as well, and so too then must the logarithm of the largest eigenvalue be. This tells us that the field $\sigma(\mathbf{x})$ is also C^2 in space and C^1 in time.

As a final note, it should be mentioned that the FTLE approach is not the only means by which LCSs may be detected within a velocity field. An alternative approach is to look at finite-size Lyapunov exponents (FSLE) (Shadden et al. (2005)). Instead of looking at how greatly two neighbouring particles separate given a finite-time period, FSLEs look at *how long* it takes two neighbouring particles to separate to a given distance. As such an approach warrants study equally as in depth as this paper, focus will remain entirely upon the FTLE here.

3. LCS Ridges

Generally speaking, LCSs are easy to locate visually within a FTLE field. They appear as a distinct ridge, thin lines of high FLTE values, dropping off sharply on either side (see figure 2). For the purpose of proving properties of the structure, however, a more exact definition is required. In fact, as per Shadden et al. (2005), we give *two* definitions, as a curvature ridge and as a second derivative ridge. These differ only in how they define the downwards direction. In the first definition, 'down' is taken to be parallel to the normal vector field of the graph (a surface in $\mathbb{R}^3$), while in the second definition 'down' is normal to the xy-plane. We define a curvature ridge as follows,

Curvature Ridge: Let $G \subset \mathbb{R}^3$ denote the graph of $\sigma : D \subset \mathbb{R}^2 \to \mathbb{R}$. Let $\pi : G \to D$ be the standard projection map, with its associated tangent map $\mathbb{T}\pi$. A curvature ridge of the graph G is an injective curve $\mathbf{c} : (a, b) \in \mathbb{R} \to D$, satisfying the following conditions for each s in the open interval (a, b):

CR1. The vectors $\mathbf{c}'(s) = \frac{d\mathbf{c}}{ds}$ and $\nabla\sigma(\mathbf{c}(s))$ are parallel.

CR2. Regard G as an orientated surface in $\mathbb{R}^3$. Let $\mathbf{p} = \mathbf{c}(s)$ and $\widetilde{\mathbf{p}} = \pi^{-1}(\mathbf{p}) \in G$. Let $k^u_{\widetilde{\mathbf{p}}}$ and $k^l_{\widetilde{\mathbf{p}}}$ denote the maximum and minimum principal curvatures of G at the point $\widetilde{\mathbf{p}}$ with corresponding unit principal vectors $\widetilde{\mathbf{u}}^u_{\widetilde{\mathbf{p}}}$ and $\widetilde{\mathbf{u}}^l_{\widetilde{\mathbf{p}}}$. We require that $k^l_{\widetilde{\mathbf{p}}} < 0$ and that $\mathbb{T}\pi(\widetilde{\mathbf{u}}^l_{\widetilde{\mathbf{p}}})$ be normal to $\mathbf{c}'(s)$

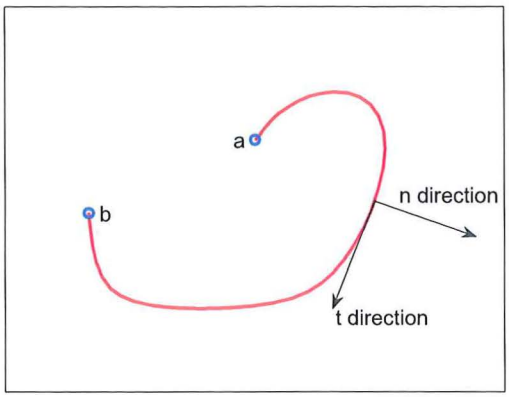

Figure 3: Injective curve c(s), where t = $\nabla\sigma$

Geometrically speaking, **CR1** conveys the property that the top of a ridgeline is flat in the transversal direction. The ridge only has slope, or a directional gradient, *along* the ridge. One has to step to the side off the ridgeline (i.e. off of $\mathbf{c}(s)$) before $\nabla\sigma(\mathbf{c}(s))$ has a directional component not alligned with $\mathbf{c}'(s)$.

Similarly, **CR2** states that the ridge drops off most steeply in the direction transverse to the ridge. It does this by looking at a point along the ridge (in the $\mathbb{R}^3$ plane), $\widetilde{\mathbf{p}}$, and considering its maximum and minimum curvatures. The minimum curvature is taken to be negative, such that $k^l_{\widetilde{\mathbf{p}}}$ must necessarily be the *most negative* curvature direction. This curvature direction is then associated with a unit principal vector, $\widetilde{\mathbf{u}}^l_{\widetilde{\mathbf{p}}}$. Mapping this unit principal vector onto the $\mathbb{R}^2$ plane, where the curve $\mathbf{c}(s)$ is found, finds that the direction of minimum (i.e. most negative) curvature is *normal* to the curve $\mathbf{c}(s)$.

Second Derivative Ridge: A second derivative ridge of σ is an injective curve $\mathbf{c} : (a, b) \to D$ satisfying the following conditions for each $s \in (a, b)$:

SR1. The vectors $\mathbf{c}'(s) = \frac{d\mathbf{c}}{ds}$ and $\nabla\sigma(\mathbf{c}(s))$ are parallel.

SR2. $\Sigma(\mathbf{n}, \mathbf{n}) = \min_{\|\mathbf{u}\|=1} \Sigma(\mathbf{u}, \mathbf{u}) < 0$, where $\mathbf{n}$ is a unit normal vector to the curve $\mathbf{c}(s)$ and Σ is thought of as a bilinear form evaluated at the point $\mathbf{c}(s)$.

Obviously **SR1** is identical to **CR1**, stating that a ridgeline is flat in the transversal direction. We also observe that **SR2** is very similar to **CR2**, in that it defines the ridgeline as having the property of dropping off most steeply (i.e. negative curvature) in the transversal direction. Instead of using the concepts of maximum and minimum curvature, however, it is phrased in terms of the Hessian, $\Sigma = \frac{d^2\sigma(\mathbf{x})}{d\mathbf{x}^2}$. **SR2** says that the second-derivative evaluated in a direction

$\mathbf{u}$ is most negative when $\mathbf{u}$ is $\mathbf{n}$, the unit normal vector to the curve $\mathbf{c}(s)$.

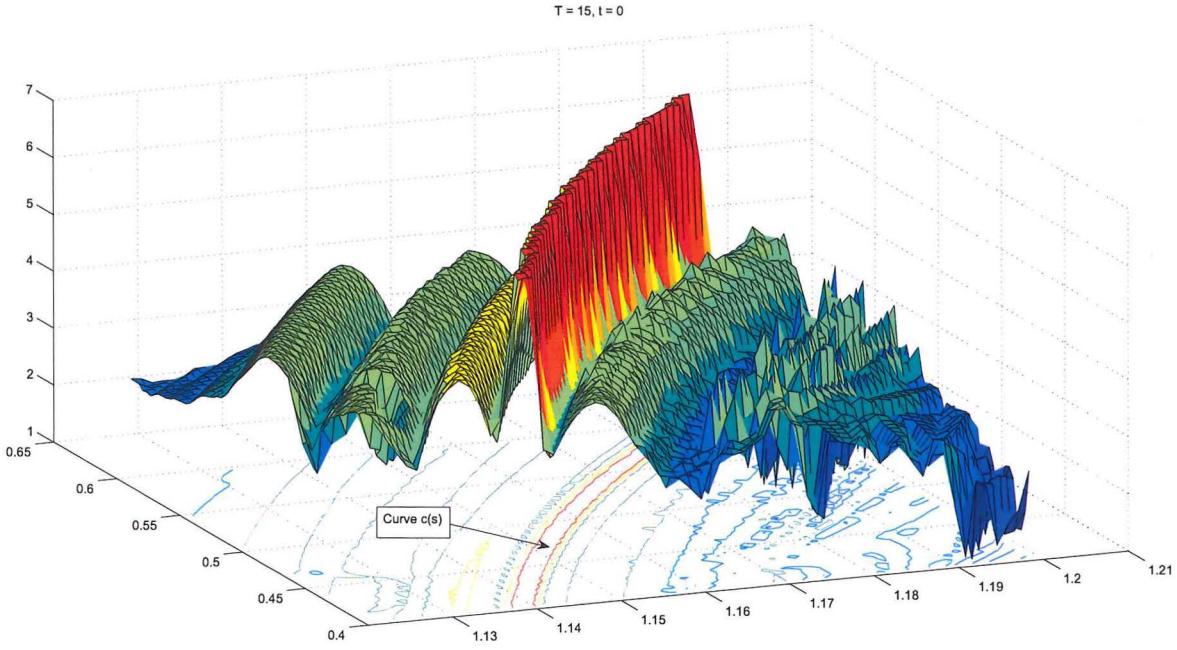

Figure 4: Enlarged view of FTLE ridge, t=0, T=15, 64x64 points

It is the curve $\mathbf{c}(s)$ that is our LCS, which may be extracted using curvature or second-derivative definitions. Yet they are not identical defintions, so one must take care in which to use. As the second-derivative definition formulates its downwards direction as normal to the xy-plane, and utilizes the more easily calculated Hessian, this choice seems more convenient, especially for numerical implementation. In fact we shall see that the second derivative ridge is a *subset* of the curvature ridge. It is therefore very useful to use the second-derivative definition, in that it will importantly never identify a ridge which the curvature definition would not have identified. First, we show the relationship between the two curvature definitions.

Let the FTLE field be given by $\sigma(\mathbf{x}) = \sigma(x, y)$, and G denote the graph of the FTLE (i.e. $z = \sigma(x, y)$). The unit normal field to G is given by $\widehat{\mathbf{u}} = \frac{1}{\kappa}\left(-\frac{\partial\sigma}{\partial x}, -\frac{\partial\sigma}{\partial y}, 1\right)$, where $\kappa = \sqrt{1 + \left(\frac{\partial\sigma}{\partial x}\right)^2 + \left(\frac{\partial\sigma}{\partial y}\right)^2}$. Next we define $\widetilde{\mathbf{n}} = (\mathbb{T}\pi)^{-1}\mathbf{n}$, which is the lift of a vector, $\mathbf{n}$, of arbitrary length and normal to $\mathbf{c}(s)$, onto G (this is the reverse of what we did in **CR2**. Note that $\mathbf{n} \to \widetilde{\mathbf{n}}$ means adding a *vertical* component, as $G \subset \mathbb{R}^3$). By definition (O'Neill (1997)), the normal curvature in the direction $\widetilde{\mathbf{n}}$ is given by $k(\widetilde{\mathbf{n}}) = \widetilde{\mathbf{n}}.\nabla_{\widetilde{\mathbf{n}}}\mathbf{u}$, where $\nabla_{\widetilde{\mathbf{n}}}\mathbf{u}$ is the covariant derivative

of $\mathbf{u}$ with respect to $\widetilde{\mathbf{n}}$. For an arbitrary vector $\mathbf{w} = (w_x, w_y, w_z)$, the curvature along $\mathbf{w}$ then is

$$\begin{aligned} k(\mathbf{w}) &= \tfrac{1}{\kappa}\left(w_x^2\tfrac{\partial^2\sigma}{\partial x^2} + 2w_xw_y\tfrac{\partial^2\sigma}{\partial x\partial y} + w_y^2\tfrac{\partial^2\sigma}{\partial y^2}\right) \\ &\quad -\tfrac{1}{\kappa^3}\left(\tfrac{\partial\sigma}{\partial x}\left(\tfrac{\partial\sigma}{\partial x}\tfrac{\partial^2\sigma}{\partial x\partial y} + \tfrac{\partial\sigma}{\partial y}\tfrac{\partial^2\sigma}{\partial y^2}\right) + \tfrac{\partial\sigma}{\partial y}\left(\tfrac{\partial\sigma}{\partial y}\tfrac{\partial^2\sigma}{\partial x\partial y} + \tfrac{\partial\sigma}{\partial x}\tfrac{\partial^2\sigma}{\partial x^2}\right)\right)w_xw_y \\ &\quad -\tfrac{1}{\kappa^3}\left(\tfrac{\partial\sigma}{\partial x}\left(\tfrac{\partial\sigma}{\partial y}\tfrac{\partial^2\sigma}{\partial x\partial y} + \tfrac{\partial\sigma}{\partial x}\tfrac{\partial^2\sigma}{\partial x^2}\right)w_x^2 + \tfrac{\partial\sigma}{\partial y}\left(\tfrac{\partial\sigma}{\partial x}\tfrac{\partial^2\sigma}{\partial x\partial y} + \tfrac{\partial\sigma}{\partial y}\tfrac{\partial^2\sigma}{\partial y^2}\right)w_y^2\right) \end{aligned} \tag{14}$$

If we plug in $\widetilde{\mathbf{n}}$ for $\mathbf{w}$, and use the fact that $\nabla\sigma.\mathbf{n} = \frac{\partial\sigma}{\partial x}n_x + \frac{\partial\sigma}{\partial y}n_y = 0$, we get

$$\begin{aligned} k(\widetilde{\mathbf{n}}) &= \tfrac{1}{\kappa}\left(n_x^2\tfrac{\partial^2\sigma}{\partial x^2} + 2n_xn_y\tfrac{\partial^2\sigma}{\partial x\partial y} + n_y^2\tfrac{\partial^2\sigma}{\partial y^2}\right) \\ &\quad -\tfrac{1}{\kappa^3}\left(\tfrac{\partial\sigma}{\partial x}\left(\tfrac{\partial\sigma}{\partial x}\tfrac{\partial^2\sigma}{\partial x\partial y} + \tfrac{\partial\sigma}{\partial y}\tfrac{\partial^2\sigma}{\partial y^2}\right) + \tfrac{\partial\sigma}{\partial y}\left(\tfrac{\partial\sigma}{\partial y}\tfrac{\partial^2\sigma}{\partial x\partial y} + \tfrac{\partial\sigma}{\partial x}\tfrac{\partial^2\sigma}{\partial x^2}\right)\right)n_xn_y \\ &\quad -\tfrac{1}{\kappa^3}\left(\tfrac{\partial\sigma}{\partial x}\left(\tfrac{\partial\sigma}{\partial y}\tfrac{\partial^2\sigma}{\partial x\partial y} + \tfrac{\partial\sigma}{\partial x}\tfrac{\partial^2\sigma}{\partial x^2}\right)n_x^2 + \tfrac{\partial\sigma}{\partial y}\left(\tfrac{\partial\sigma}{\partial x}\tfrac{\partial^2\sigma}{\partial x\partial y} + \tfrac{\partial\sigma}{\partial y}\tfrac{\partial^2\sigma}{\partial y^2}\right)n_y^2\right) \\ &= \tfrac{1}{\kappa}\left(n_x^2\tfrac{\partial^2\sigma}{\partial x^2} + 2n_xn_y\tfrac{\partial^2\sigma}{\partial x\partial y} + n_y^2\tfrac{\partial^2\sigma}{\partial y^2}\right) \\ &\quad -\tfrac{n_x}{\kappa^3}\tfrac{\partial\sigma}{\partial x}\left(\tfrac{\partial^2\sigma}{\partial x\partial y}\left(n_y\tfrac{\partial\sigma}{\partial x} + n_x\tfrac{\partial\sigma}{\partial y}\right)\right) - \tfrac{n_y}{\kappa^3}\tfrac{\partial\sigma}{\partial y}\left(\tfrac{\partial^2\sigma}{\partial x\partial y}\left(n_y\tfrac{\partial\sigma}{\partial x} + n_x\tfrac{\partial\sigma}{\partial y}\right)\right) \\ &\quad -\tfrac{n_x}{\kappa^3}\tfrac{\partial\sigma}{\partial x}\left(n_y\left(\tfrac{\partial\sigma}{\partial y}\tfrac{\partial^2\sigma}{\partial y^2}\right) + n_x\left(\tfrac{\partial\sigma}{\partial x}\tfrac{\partial^2\sigma}{\partial x^2}\right)\right) - \tfrac{n_y}{\kappa^3}\tfrac{\partial\sigma}{\partial y}\left(n_y\left(\tfrac{\partial\sigma}{\partial y}\tfrac{\partial^2\sigma}{\partial y^2}\right) + n_x\left(\tfrac{\partial\sigma}{\partial x}\tfrac{\partial^2\sigma}{\partial x^2}\right)\right) \\ &= \tfrac{1}{\kappa}\left(n_x^2\tfrac{\partial^2\sigma}{\partial x^2} + 2n_xn_y\tfrac{\partial^2\sigma}{\partial x\partial y} + n_y^2\tfrac{\partial^2\sigma}{\partial y^2}\right) \\ &\quad \left(\tfrac{\partial\sigma}{\partial x}n_x + \tfrac{\partial\sigma}{\partial y}n_y\right)\tfrac{-1}{\kappa^3}\left(\tfrac{\partial^2\sigma}{\partial x\partial y}\left(n_y\tfrac{\partial\sigma}{\partial x} + n_x\tfrac{\partial\sigma}{\partial y}\right)\right) \\ &\quad \left(\tfrac{\partial\sigma}{\partial x}n_x + \tfrac{\partial\sigma}{\partial y}n_y\right)\tfrac{-1}{\kappa^3}\left(n_y\left(\tfrac{\partial\sigma}{\partial y}\tfrac{\partial^2\sigma}{\partial y^2}\right) + n_x\left(\tfrac{\partial\sigma}{\partial x}\tfrac{\partial^2\sigma}{\partial x^2}\right)\right) \\ &= \tfrac{1}{\kappa}\left(n_x^2\tfrac{\partial^2\sigma}{\partial x^2} + 2n_xn_y\tfrac{\partial^2\sigma}{\partial x\partial y} + n_y^2\tfrac{\partial^2\sigma}{\partial y^2}\right) = \tfrac{1}{\kappa}\Sigma(\mathbf{n},\mathbf{n}) \end{aligned} \tag{15}$$

Similarly, let $\mathbf{t}$ be a vector of arbitrary length oriented along $\nabla\sigma$ (if $\nabla\sigma = 0$ then $\mathbf{t}$ may be arbitrarily oriented). If we plug in $\widetilde{\mathbf{t}} = \mathbf{u}$ x $\widetilde{\mathbf{n}}$ for $\mathbf{w}$, and define $k(\widetilde{\mathbf{t}}) = \widetilde{\mathbf{t}}.\nabla_{\widetilde{\mathbf{t}}}\mathbf{u}$, then we find (after some lengthy algebra)

$$k(\widetilde{\mathbf{t}}) = \tfrac{1}{\kappa^3}\left(t_x^2\tfrac{\partial^2\sigma}{\partial x^2} + 2t_xt_y\tfrac{\partial^2\sigma}{\partial x\partial y} + t_y^2\tfrac{\partial^2\sigma}{\partial y^2}\right) = \tfrac{1}{\kappa^3}\Sigma(\mathbf{t},\mathbf{t}) \tag{16}$$

Thus we are left with the relations,

$$\Sigma(\mathbf{n},\mathbf{n}) = \kappa k(\widetilde{\mathbf{n}}) \tag{17}$$

$$\Sigma(\mathbf{t},\mathbf{t}) = \kappa^3 k(\widetilde{\mathbf{t}})$$

It should be easily observed that $\kappa \geq 1$, by definition. A direct consequence, then, is that the two curvature definitions are exactly equal only where $\kappa = 1$, which implies that $\nabla\sigma = 0$.

This special case has the tangent plane of G parallel to the xy-plane, such that the ridge is entirely flat in all directions.

Let us move on to show that a second derivative ridge is identical to or a subset of a curvature ridge. We must show that if **CR1** and **CR2** are satisfied, then so are **SR1** and **SR2**. Obviously this is true for **CR1** and **SR1**, as they are identical. Next we require **CR2** to be true, that $k(\widetilde{\mathbf{n}})$ is the most negative curvature direction, where $\widetilde{\mathbf{n}}$ is the lift of $\mathbf{n}$, and $\mathbf{n}$ satisfies $\Sigma(\mathbf{n},\mathbf{n}) = \min_{\|\mathbf{u}\|=1} \Sigma(\mathbf{u},\mathbf{u}) < 0$, with $\mathbf{n}$ orthogonal to $\nabla\sigma$.

By the curvature relation for $\widetilde{\mathbf{n}}$ in (17), if $\Sigma(\mathbf{n},\mathbf{n}) < 0$ then $k(\widetilde{\mathbf{n}}) < 0$ also, as $\kappa > 0$. Therefore we just need to prove that $k(\widetilde{\mathbf{n}})$ is minimized (i.e. most negative) in the $\widetilde{\mathbf{n}}$ direction, orthogonal to the second-derivative ridge. Obviously if $\widetilde{\mathbf{n}}$ is the only direction of negative curvature, this is trivially satisfied. Only where the eigenvalues of Σ satisfy $\lambda_{\min} < \lambda_{\max} < 0$ do we still need to prove anything. Without loss of generality, we can assume the second-derivative ridge is locally aligned with the x-axis, such that $\frac{\partial\sigma}{\partial y} = 0$. This puts Σ into canonical form,

$$\Sigma = \begin{bmatrix} \frac{\partial^2\sigma}{\partial x^2} & \frac{\partial^2\sigma}{\partial x \partial x} \\ \frac{\partial^2\sigma}{\partial x \partial x} & \frac{\partial^2\sigma}{\partial y^2} \end{bmatrix} = \begin{bmatrix} \frac{\partial^2\sigma}{\partial x^2} & 0 \\ 0 & \frac{\partial^2\sigma}{\partial y^2} \end{bmatrix} = \begin{bmatrix} \lambda_{\max} & 0 \\ 0 & \lambda_{\min} \end{bmatrix} \tag{18}$$

If we use this relation in (14) with $\widehat{\mathbf{u}}$ as an arbitrary unit vector $(u_x, u_y, 0)$, we find

$$\begin{aligned} k(\widehat{\mathbf{u}}) &= \tfrac{1}{\kappa}\left(u_x^2\tfrac{\partial^2\sigma}{\partial x^2} + 2u_xu_y\tfrac{\partial^2\sigma}{\partial x\partial y} + u_y^2\tfrac{\partial^2\sigma}{\partial y^2}\right) \\ &\quad -\tfrac{1}{\kappa^3}\left(\tfrac{\partial\sigma}{\partial x}\left(\tfrac{\partial\sigma}{\partial x}\tfrac{\partial^2\sigma}{\partial x\partial y} + \tfrac{\partial\sigma}{\partial y}\tfrac{\partial^2\sigma}{\partial y^2}\right) + \tfrac{\partial\sigma}{\partial y}\left(\tfrac{\partial\sigma}{\partial y}\tfrac{\partial^2\sigma}{\partial x\partial y} + \tfrac{\partial\sigma}{\partial x}\tfrac{\partial^2\sigma}{\partial x^2}\right)\right)u_xu_y \\ &\quad -\tfrac{1}{\kappa^3}\left(\tfrac{\partial\sigma}{\partial x}\left(\tfrac{\partial\sigma}{\partial y}\tfrac{\partial^2\sigma}{\partial x\partial y} + \tfrac{\partial\sigma}{\partial x}\tfrac{\partial^2\sigma}{\partial x^2}\right)u_x^2 + \tfrac{\partial\sigma}{\partial y}\left(\tfrac{\partial\sigma}{\partial x}\tfrac{\partial^2\sigma}{\partial x\partial y} + \tfrac{\partial\sigma}{\partial y}\tfrac{\partial^2\sigma}{\partial y^2}\right)u_y^2\right) \\ &= \tfrac{1}{\kappa}\left(u_x^2\tfrac{\partial^2\sigma}{\partial x^2} + u_y^2\tfrac{\partial^2\sigma}{\partial y^2}\right) - \tfrac{1}{\kappa^3}\left(\tfrac{\partial\sigma}{\partial x}\left(\tfrac{\partial\sigma}{\partial x}\tfrac{\partial^2\sigma}{\partial x^2}\right)u_x^2\right) \\ &= \tfrac{1}{\kappa}\left(u_x^2\lambda_{\max} + u_y^2\lambda_{\min}\right) - \tfrac{1}{\kappa^3}\left(|\nabla\sigma|^2\lambda_{\max}u_x^2\right) \end{aligned} \tag{19}$$

Minimizing this equation is rather simple; κ is positive and greater than zero, such that the third term is small and positive ($\lambda_{\max} < 0$). The first two terms are both negative, but since $\lambda_{\min} < \lambda_{\max}$, the equation is minimized where $\widehat{\mathbf{u}} = (0,1,0)$. Hence $k(\widehat{\mathbf{u}})$ is minimized if $\widehat{\mathbf{u}}$ is in the y-direction, which is orthogonal to the second-derivative ridge, and so we have proven that **CR2** is true if **SR2** is. Based on our work here, we now define the following:

Lagrangian Coherent Structure: At each time t, a Lagrangian coherent structure (LCS) is a second-derivative ridge of the scalar field $\sigma_{t_0}^{t_0+T}(\mathbf{x})$.

While the second-derivative ridge is only a subset of the curvature ridge, generally the two are almost identical. In most FTLE fields, σ does not vary much along a ridge (see figure 4), so little in fact that there is practically no difference between measures. For autonomous systems we can even show that the two measures are identical. We do this by showing that σ is constant along the ridge (asymptotically), which gives the previously mentioned special case of $\nabla\sigma = 0$.

Let us compare the value of the FTLE computed for two different points in time along the *same trajectory.* For the sake of simplicity, set $t_0 = 0$ as the time along a given trajectory where a particle is at position $\mathbf{x}$, and $\mathbf{y}$ as the position of the particle s time units later (i.e. $\mathbf{y} = \phi_0^s(\mathbf{x})$ for some $s \in \mathbb{R}$). This gives

$$\begin{aligned}
|T|(\sigma_0^T(\mathbf{x}) - \sigma_s^{s+T}(\mathbf{y})) &= \ln\left\|\frac{d\phi_{t_0}^T(\mathbf{x})}{d\mathbf{x}}\right\| - \ln\left\|\frac{d\phi_s^{s+T}(\mathbf{y})}{d\mathbf{y}}\right\| \\
&= \ln\left\|\frac{d(\phi_{T+s}^T(\phi_T^{T+s}(\phi_s^T(\phi_0^s(\mathbf{x})))))}{d\mathbf{x}}\right\| - \ln\left\|\frac{d(\phi_T^{s+T}(\phi_s^T(\mathbf{y})))}{d\mathbf{y}}\right\| \\
&= \ln\left\|\frac{d\phi_{T+s}^T(\widehat{\mathbf{y}})}{d\widehat{\mathbf{y}}}\frac{d\phi_T^{T+s}(\widehat{\mathbf{x}})}{d\widehat{\mathbf{x}}}\frac{d\phi_s^T(\mathbf{y})}{d\mathbf{y}}\frac{d\phi_0^s(\mathbf{x})}{d\mathbf{x}}\right\| - \ln\left\|\frac{d\phi_T^{s+T}(\widehat{\mathbf{x}})}{d\widehat{\mathbf{x}}}\frac{d\phi_s^T(\mathbf{y})}{d\mathbf{y}}\right\| \\
&\leq \ln\left(\left\|\frac{d\phi_{T+s}^T(\widehat{\mathbf{y}})}{d\widehat{\mathbf{y}}}\right\|\left\|\frac{d\phi_T^{T+s}(\widehat{\mathbf{x}})}{d\widehat{\mathbf{x}}}\frac{d\phi_s^T(\mathbf{y})}{d\mathbf{y}}\right\|\left\|\frac{d\phi_0^s(\mathbf{x})}{d\mathbf{x}}\right\|\right) - \ln\left\|\frac{d\phi_T^{s+T}(\widehat{\mathbf{x}})}{d\widehat{\mathbf{x}}}\frac{d\phi_s^T(\mathbf{y})}{d\mathbf{y}}\right\| \\
&= \ln\left\|\frac{d\phi_{T+s}^T(\widehat{\mathbf{y}})}{d\widehat{\mathbf{y}}}\right\| + \ln\left\|\frac{d\phi_0^s(\mathbf{x})}{d\mathbf{x}}\right\| \\
&\leq k|T - (T+s)| + k|s - 0| = 2k|s|
\end{aligned} \tag{20}$$

Where we have used (12), the exponential stretching hypothesis, as well as basic flow map properties (4). In a similar manner, we find

$$|T|(\sigma_s^{s+T}(\mathbf{y}) - \sigma_0^T(\mathbf{x})) \leq 2k|s| \tag{21}$$

Together these give

$$\| \sigma_0^T(\mathbf{x}) - \sigma_s^{s+T}(\mathbf{y}) \| \leq 2k\frac{|s|}{|T|} \tag{22}$$

And so if we take the limit as $s \to 0$, we get

$$\left\| \frac{d\phi_t^T(\mathbf{x})}{dt} \right\| =_{s\to 0} \frac{\| \sigma_{t+s}^{s+T}(\mathbf{y}) - \sigma_t^T(\mathbf{x}) \|}{|s|} \leq \frac{2k}{|T|} = O(1/|T|) \tag{23}$$

Taking the limit as $|T| \to \infty$ gives

$$\lim_{|T|\to\infty} \sup \left\| \frac{d\phi_t^T(\mathbf{x})}{dt} \right\| = 0 \tag{24}$$

Which implies that σ is asymptotically constant along the ridge, i.e.

$$\lim_{|T|\to\infty} \left\| \frac{d\phi_t^T(\mathbf{x})}{dt} \right\| = 0 \tag{25}$$

4. Level Sets

Our purpose now will be to move towards an estimate for the flux across the LCS. Ideally this should be zero, if the LCS is fully Lagrangian. However we shall soon see that these structures are generally only approximately Lagrangian. Our approach will be to first define a function $L(\mathbf{x}, t)$, such that the LCS is given by the level set $L(\mathbf{x}, t) = 0$, from which we can derive an expression for DL/Dt. We are then able to give the flux through the LCS at any point along its length (assuming it has infinitesimal width, ds), by

$$d\Phi = \left. \frac{DL}{Dt} \right|_{L=0} ds \tag{26}$$

where the derivative on the RHS is the material derivative, $\frac{DL}{Dt}$, of the scalar level set.

Given an FTLE field $\sigma_t^T(\mathbf{x})$ where $t \in [t_1, t_2]$, and which an LCS can be found for, we define a scalar function L as follows:

Level Set: For every time t, let $L(\mathbf{x}, t)$ be the function of $\mathbf{x} \in D$ defined by the conditions

L1. $|L(\mathbf{x}, t)| = \| \mathbf{x} - \mathbf{x}_q \|$, where $\mathbf{x}_q$ is the point on the LCS closest to $\mathbf{x}$.

L2. $L(\mathbf{x}, t)(((\mathbf{x} - \mathbf{x}_q) \times \mathbf{c}_t'(s)) \cdot \widehat{\mathbf{k}}) \geq 0$.

where $\widehat{\mathbf{k}}$ is the unit basis vector pointing 'up' from the domain D. Therefore $L(\mathbf{x}, t)$ simply gives the signed distance from $\mathbf{x}$ to the closest point on the LCS. Moving along the curve $\mathbf{c}(s)$ in the positive $\mathbf{c}'(s)$ direction gives points on the immediate right a positive sign, and negative

sign for those on the left.

It should be obvious by the above definition that $\nabla L = \hat{\mathbf{n}}(\mathbf{x}, t)$, where $\hat{\mathbf{n}}(\mathbf{x}, t)$ is a unit vector parallel to $\mathbf{x} - \mathbf{x}_q$. There is no change in the level set in the direction tangential to the LCS; only in the direction normal to the curve does L vary. Let us define the unit vector orthogonal to $\hat{\mathbf{n}}$ as $\hat{\mathbf{t}} = \hat{\mathbf{k}}$ x $\hat{\mathbf{n}}$. $\hat{\mathbf{t}}$ corresponds with the direction tangential to the LCS, and as such is parallel to $\nabla\sigma$. The two are not identical, however, as $\nabla\sigma$ may be oriented in the $\mathbf{c}'(s)$ or $-\mathbf{c}'(s)$ directions, or possibly even be equal to zero. For these reasons we work with $\hat{\mathbf{t}}$ preferentially.

Along the LCS level set, where $L = 0$, we are able to derive some useful relations between $\hat{\mathbf{n}}$ and $\hat{\mathbf{t}}$. **SR2** implies that $\hat{\mathbf{n}}$ is an eigenvector of Σ, corresponding with the most negative eigenvalue (in a similar manner to equation (18)). Hence, $\langle\hat{\mathbf{t}}, \Sigma\hat{\mathbf{n}}\rangle = \lambda_{\min}(\Sigma)\langle\hat{\mathbf{t}}, \hat{\mathbf{n}}\rangle = 0$, where $\lambda_{\min}(\Sigma)$ is the most negative eigenvalue of Σ. Therefore we find that for $L = 0$, $\langle\hat{\mathbf{t}}, \Sigma\hat{\mathbf{n}}\rangle = \langle\hat{\mathbf{n}}, \Sigma\hat{\mathbf{t}}\rangle = 0$.

Next, consider an arbitrary vector $\mathbf{v}$, which we represent in the orthonormal basis $(\hat{\mathbf{t}}, \hat{\mathbf{n}})$. This gives us $\mathbf{v} = \langle\hat{\mathbf{t}}, \mathbf{v}\rangle\hat{\mathbf{t}} + \langle\hat{\mathbf{n}}, \mathbf{v}\rangle\hat{\mathbf{n}}$, and so $\Sigma\mathbf{v} = \langle\hat{\mathbf{t}}, \mathbf{v}\rangle\Sigma\hat{\mathbf{t}} + \langle\hat{\mathbf{n}}, \mathbf{v}\rangle\Sigma\hat{\mathbf{n}}$. Since we have already shown that $\langle\hat{\mathbf{n}}, \Sigma\hat{\mathbf{t}}\rangle = 0$, we therefore find that $\langle\hat{\mathbf{n}}, \Sigma\mathbf{v}\rangle = \langle\hat{\mathbf{n}}, \mathbf{v}\rangle\langle\hat{\mathbf{n}}, \Sigma\hat{\mathbf{n}}\rangle$.

We only need prove two more pieces before we are able to put together an expression for DL/Dt. First, consider $\mathbf{x}$ and $\mathbf{y}$, where $\mathbf{x}$ is on the LCS at time t, and $\mathbf{y} = \mathbf{x} + \alpha(\delta t)\hat{\mathbf{n}}$ is on the LCS at time $t + \delta t$. This $\mathbf{y}$, then, is located on the intersection of the LCS at time $t + \delta t$, and a line of some unknown length, which begins at $\mathbf{x}$ and is orthogonal to the LCS at time t. As $\mathbf{x} = \mathbf{y}$ for $\delta t = 0$, it follows that $\alpha(\delta t)$ is $O(\delta t)$. We now take a second-order expansion of $L(\mathbf{y}, t + \delta t) = 0$,

$$\begin{aligned} 0 \;=\; L(\mathbf{y}, t+\delta t) \;&=\; L(\mathbf{x}, t) + \alpha + \tfrac{\partial L}{\partial t}\delta t + O(\delta t^2) \\ &=\; \alpha + \tfrac{\partial L}{\partial t}\delta t + O(\delta t^2) \qquad (27) \\ \alpha \;&=\; -\tfrac{\partial L}{\partial t}\delta t + O(\delta t^2) \end{aligned}$$

Now we expand ∇L, using the fact that $\mathcal{L}\hat{\mathbf{n}} = 0$, where $\mathcal{L}$ is the Hessian of L (see Appendix 2).

$$\nabla L|_{\mathbf{y}, t+\delta t} = \nabla L + \frac{\partial \nabla L}{\partial t}\delta t + O(\delta t^2) \qquad (28)$$

Next we apply a similar expansion for $\nabla\sigma$, then plug in our expression for α

$$\begin{aligned} \nabla\sigma|_{\mathbf{y},t+\delta t} &= \nabla\sigma + \alpha\Sigma\widehat{\mathbf{n}} + \tfrac{\partial\nabla\sigma}{\partial t}\delta t + O(\delta t^2) \\ &= \nabla\sigma - \tfrac{\partial L}{\partial t}\Sigma\nabla L\delta t + \tfrac{\partial\nabla\sigma}{\partial t}\delta t + O(\delta t^2) \end{aligned} \tag{29}$$

Since $\mathbf{y}$ is on the LCS at time $t+\delta t$, (28) and (29) are orthogonal, and so

$$\begin{aligned} 0 &= \langle \nabla L|_{\mathbf{y},t+\delta t}\,,\, \nabla\sigma|_{\mathbf{y},t+\delta t}\rangle \\ &= \langle\nabla L, \nabla\sigma\rangle + \delta t\left(-\tfrac{\partial L}{\partial t}\langle\nabla L, \Sigma\nabla L\rangle + \tfrac{\partial\langle\nabla L,\nabla\sigma\rangle}{\partial t}\right) + O(\delta t^2) \\ &= \delta t\left(-\langle\widehat{\mathbf{n}}, \Sigma\widehat{\mathbf{n}}\rangle\tfrac{\partial L}{\partial t} + \tfrac{\partial\langle\widehat{\mathbf{n}},\nabla\sigma\rangle}{\partial t}\right) + O(\delta t^2) \end{aligned} \tag{30}$$

As δt is small, $O(\delta t^2)$ terms are negligible, and so for $L = 0$ we find that

$$\langle\widehat{\mathbf{n}}, \Sigma\widehat{\mathbf{n}}\rangle\frac{\partial L}{\partial t} = \frac{\partial\langle\widehat{\mathbf{n}}, \nabla\sigma\rangle}{\partial t} \tag{31}$$

Lastly, from equation (23) we know that the material derivative of σ satisfies $\frac{D\sigma}{Dt} = O(1/|T|)$, giving

$$\frac{\partial\sigma}{\partial t} = -\langle\mathbf{v}, \nabla\sigma\rangle + O(1/|T|) \tag{32}$$

Since we've already established that $\nabla\sigma$ is C^1 in time, we have $|\frac{\partial\nabla\sigma}{\partial t}| < \infty$. Therefore by the spatial derivative of (32) we find

$$\frac{\partial\nabla\sigma}{\partial t} = \nabla\frac{\partial\sigma}{\partial t} = -\nabla\langle\mathbf{v}, \nabla\sigma\rangle + O(1/|T|) \tag{33}$$

Using suffix notation, we can rewrite as follows

$$\begin{aligned} \tfrac{\partial\nabla\sigma}{\partial t} &= -\partial_i(v_j\partial_j\sigma) + O(1/|T|) \\ &= -(\partial_i v_j)\partial_j\sigma - (\partial_i\partial_j\sigma)v_j + O(1/|T|) \\ &= -J * \nabla\sigma - \Sigma\mathbf{v} + O(1/|T|) \end{aligned} \tag{34}$$

This gives us all we need to construct a formula for the flux across the LCS, DL/Dt. Consider the material derivative for L, to which we then apply equation (31).

$$\begin{aligned} \frac{DL}{Dt} &= \frac{\partial L}{\partial t} + \mathbf{v} \cdot \nabla L \\ \langle \hat{\mathbf{n}}, \Sigma\hat{\mathbf{n}} \rangle \frac{DL}{Dt} &= \langle \hat{\mathbf{n}}, \Sigma\hat{\mathbf{n}} \rangle \frac{\partial L}{\partial t} + \langle \hat{\mathbf{n}}, \Sigma\hat{\mathbf{n}} \rangle \langle \mathbf{v}, \hat{\mathbf{n}} \rangle \\ &= \frac{\partial \langle \hat{\mathbf{n}}, \nabla\sigma \rangle}{\partial t} + \langle \hat{\mathbf{n}}, \Sigma\hat{\mathbf{n}} \rangle \langle \mathbf{v}, \hat{\mathbf{n}} \rangle \end{aligned} \tag{35}$$

Next we apply the chain rule for the derivative, and simplify the second term on the right-hand side as earlier described,

$$\langle \hat{\mathbf{n}}, \Sigma\hat{\mathbf{n}} \rangle \frac{DL}{Dt} = \left\langle \nabla\sigma, \frac{\partial \hat{\mathbf{n}}}{\partial t} \right\rangle + \left\langle \hat{\mathbf{n}}, \frac{\partial \nabla\sigma}{\partial t} \right\rangle + \langle \hat{\mathbf{n}}, \Sigma\mathbf{v} \rangle \tag{36}$$

We then plug in equation (34), then use the substitution $\nabla\sigma = \langle \hat{\mathbf{t}}, \nabla\sigma \rangle \hat{\mathbf{t}}$ (i.e. $\hat{\mathbf{t}}$ is proportional to $\nabla\sigma$).

$$\begin{aligned} \langle \hat{\mathbf{n}}, \Sigma\hat{\mathbf{n}} \rangle \frac{DL}{Dt} &= \left\langle \nabla\sigma, \frac{\partial \hat{\mathbf{n}}}{\partial t} \right\rangle + \langle \hat{\mathbf{n}}, -J * \nabla\sigma - \Sigma\mathbf{v} \rangle + \langle \hat{\mathbf{n}}, \Sigma\mathbf{v} \rangle + O(1/|T|) \\ &= \left\langle \nabla\sigma, \frac{\partial \hat{\mathbf{n}}}{\partial t} \right\rangle + \langle \hat{\mathbf{n}}, -J * \nabla\sigma \rangle - \langle \hat{\mathbf{n}}, \Sigma\mathbf{v} \rangle + \langle \hat{\mathbf{n}}, \Sigma\mathbf{v} \rangle + O(1/|T|) \\ &= \left\langle \nabla\sigma, \frac{\partial \hat{\mathbf{n}}}{\partial t} \right\rangle + \langle \hat{\mathbf{n}}, -J * \nabla\sigma \rangle + O(1/|T|) \\ &= \left\langle \nabla\sigma, \frac{\partial \hat{\mathbf{n}}}{\partial t} - J\hat{\mathbf{n}} \right\rangle + O(1/|T|) \\ &= \langle \hat{\mathbf{t}}, \nabla\sigma \rangle \left\langle \hat{\mathbf{t}}, \frac{\partial \hat{\mathbf{n}}}{\partial t} - J\hat{\mathbf{n}} \right\rangle + O(1/|T|) \end{aligned} \tag{37}$$

This gives us our final result,

$$\frac{DL}{Dt} = \frac{\langle \hat{\mathbf{t}}, \nabla\sigma \rangle}{\langle \hat{\mathbf{n}}, \Sigma\hat{\mathbf{n}} \rangle} \left\langle \hat{\mathbf{t}}, \frac{\partial \hat{\mathbf{n}}}{\partial t} - J\hat{\mathbf{n}} \right\rangle + O(1/|T|) \tag{38}$$

Let us consider what each part of the above equation means, starting with $\frac{\langle \hat{\mathbf{t}}, \nabla\sigma \rangle}{\langle \hat{\mathbf{n}}, \Sigma\hat{\mathbf{n}} \rangle}$. The numerator, $\langle \hat{\mathbf{t}}, \nabla\sigma \rangle$, is a measure of how greatly the LCS varies as you move along it. It is equivalent to $\| \nabla\sigma \|$, which means that for LCSs that vary little along the ridgeline, the numerator is small. In fact we have already seen that for autonomous systems $\nabla\sigma = 0$ (asymptotically), and therefore the numerator is zero. The flux in this case is zero, as both terms are

zero, since $O(1/|T|) \to 0$ as $t \to \infty$. Of course this is expected, as in these cases we expect to find proper invariant manifolds. Generally σ does not vary much even for non-autonomous systems, such that we expect the numerator to be small.

The denominator, $\langle \widehat{\mathbf{n}}, \Sigma\widehat{\mathbf{n}} \rangle$, measures how sharply the ridgeline slopes in the orthogonal direction. This we would expect to be large, as we have already found this quantity to be less than zero and (locally) minimized (i.e. its norm is maximized). In fact, the steeper the slope of the ridge, the greater the denominator, and the smaller the flux. Poorly defined ridgelines, on the other hand, will have a smaller denominator, and so exhibit greater flux. The denominator and numerator together can be thought of as a *structural* requirement, that the LCS is well-defined from the rest of the field, and that it doesn't vary too greatly along its length.

Next we consider $\left\langle \widehat{\mathbf{t}}, \frac{\partial \widehat{\mathbf{n}}}{\partial t} - J\widehat{\mathbf{n}} \right\rangle$. The first part, $\left\langle \widehat{\mathbf{t}}, \frac{\partial \widehat{\mathbf{n}}}{\partial t} \right\rangle$, is a measure of how fast the LCS is locally rotating, which we term a *Lagrangian rotation.* A nicer way of interpreting this term than direct inspection (though this should still be sufficiently clear), is to make the substitutions $\widehat{\mathbf{n}} = (\cos\theta, \sin\theta)$ and $\widehat{\mathbf{t}} = (-\sin\theta, \cos\theta)$ for an appropriate θ. This lets us rewrite as

$$\left\langle \widehat{\mathbf{t}}, \frac{\partial \widehat{\mathbf{n}}}{\partial t} \right\rangle = \begin{bmatrix} -\sin\theta & \cos\theta \end{bmatrix} \begin{bmatrix} -\dot{\theta}\sin\theta \\ \dot{\theta}\cos\theta \end{bmatrix} = \dot{\theta} \tag{39}$$

Now, $J\widehat{\mathbf{n}}$ is the linearized velocity field as applied to a unit vector normal to the LCS. Taking the inner product of this with the unit vector tangent to the LCS, $\widehat{\mathbf{t}}$, gives the component in the direction of the LCS. This means that $\left\langle \widehat{\mathbf{t}}, J\widehat{\mathbf{n}} \right\rangle$ measures how much the local Eulerian field rotates vectors normal to the LCS, which we term the *Eulerian rotation.* Hence, $\left\langle \widehat{\mathbf{t}}, \frac{\partial \widehat{\mathbf{n}}}{\partial t} - J\widehat{\mathbf{n}} \right\rangle$ measures the difference between Lagrangian and Eulerian rotation rates. If the LCS rotates in sync with the velocity field, then this term is zero, and the only flux is $O(1/|T|)$. But if these two are not equal, such as due to a sudden increase or decrease of the local vorticity in the field, the flux increases. This can be thought of as a *coherency* requirement for the LCS, in that if its rotation rate doesn't match that of the velocity field, then it is not being transported as a coherent structure within that field.

The final term is $O(1/|T|)$, which of course decreases as time increases. If integration time, T, is very small, then this last term (and consequently the flux) will be large. This should be expected, as an instantaneous FTLE is of little use in determining where an LCS is located. The FTLE measures the largest degree of separation over a given time period, so particles need sufficient time to separate in order for the FTLE to discriminate between those close to an LCS and those not. Such a requirement (i.e. large T) puts a practical limitation on the use of the FTLE method for locating LCSs, in that T values can often only be chosen within a certain range. Overly large values can drastically increase computation time, or can be pure nonsense when equations are known only for a finite time period. This is particularly so when source

data is experimentally gathered. We shall discuss this issue more in the next section.

For an LCS to be approximately Lagrangian, which is to say that the flux across the structure is negligible, there are certain criteria to be met. These we have found based on our equation (38). It must (a) have a sufficiently level ridgeline, (b) slope sharply downwards on either side of the ridgeline, (c) rotate at a rate similar to that induced by the velocity field, and (d) be computed for a sufficiently large integration time. Let us move now to numerical implementation of the theory we have built up, and see how it holds up in practice.

5. Computation & Interpretation

As of yet we have not moved into a discussion of how to implement the ideas we have developed, and with good reason. Most crucially, one needs to realise that computing FTLE fields is computationally expensive, requiring the integration of a large number of points over a given time period. This means that we have to consider carefully issues of accuracy and computation time before we think of running any programs. The next most important issue is that we need be aware of the nature of the information we are getting back from any fields we have computed. Non-autonomous systems are those which depend on time, and as such an LCS also depends on time. We shall return to this point soon; for now let us begin with the construction of our numerical algorithm.

To compute the FTLE field, as per equation (11), first requires computation of $\frac{d\phi_{t_0}^{t_0+T}(\mathbf{x})}{d\mathbf{x}}$, the gradient of the flow map. This is done by a technique called finite differencing, of which we use the *central* difference method. Here we take four points evenly spaced around $\mathbf{x}$ (i.e. above, below, to the left and to the right), and look at how their distance from $\mathbf{x}$ changes as they are advected by the flow over the integration time, T.

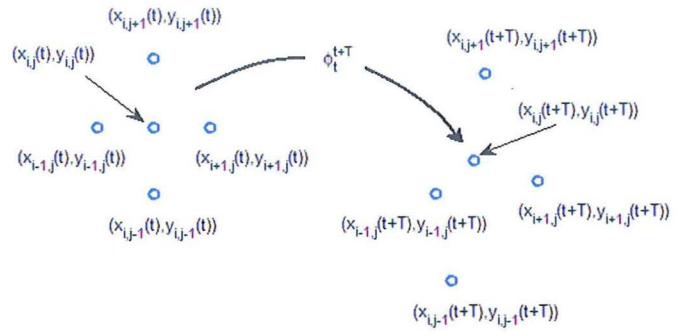

Figure 5: The deformation tensor maps a blob of points around $\mathbf{x}$

In this manner we define the matrix D for each $\mathbf{x}$ as

$$D = \begin{bmatrix} \frac{\delta\sigma_x}{\delta x} & \frac{\delta\sigma_x}{\delta y} \\ \frac{\delta\sigma_y}{\delta x} & \frac{\delta\sigma_y}{\delta y} \end{bmatrix} \tag{40}$$

where $\delta\sigma_x$ is horizontal separation of the left and right points after advection by the flow, $\delta\sigma_y$ is vertical separation of top and bottom points after advection by the flow, and δx and δy are initial horizontal and vertical separation of points respectively. These last two are equal to the spacing of the grid used for the field. Remember that what we are calculating here is a finite time version of the Cauchy-Green deformation tensor; what our algorithm needs to do is look at how a blob of particles around a point deforms as the system evolves. Therefore $\delta\sigma_x$ and $\delta\sigma_y$ require the computation of $\mathbf{x}_{t+T} = \phi_t^{t+T}(\mathbf{x})$, for which we use a fourth-order Runge-Kutta-Fehlberg solver, which is standard for many applications. Note that if data is experimentally derived, an interpolator is first required, generally third-order. It is this step, computing $\phi_t^{t+T}(\mathbf{x})$, that takes the bulk of the computation time for our FTLE code, as this step must be done for *every point in the field*, which can be very numerous indeed. In the example below, we compute the FTLE field for a grid of 1024 x 512 points with $T = 15$, which means 524, 288 unique points (grid spacing = 0.002). This first step in our algorithm alone takes approximately 50 minutes to run, given such a grid. Halving the grid spacing would quadruple the time taken, to more than 3 hrs!

Now that we have computed the matrix D (for each point $\mathbf{x}$ in the field), we take the 2-norm of the matrix, then take the log of the result. By equation (11) we should next multiply by $1/|T|$, but this is simply a method of scaling the field according to the integration time. The result would be to provide the *average* separation of particles, useful for comparing FTLE plots for different systems. If we simply wish to look at the structure of the field, rather than use the FTLE for any calculations or system comparisons, then it is simpler to leave out this scaling. However, if we are attempting to calculate the flux, then we do need correct FTLE values, scaling by time. Our FTLE example shall use the unscaled version for $\sigma(\mathbf{x})$. Appendix 3 gives a selection of MATLAB code used in carrying out this computation.

How to choose T is difficult to give any firm answer to. Computation of FTLE fields from experimental data are limited by the time frame of source data, especially where a series of FTLE fields are required (i.e. for a series of t values). However, even where not limited by availability of data, T should not be chosen to be too large. Overly large choices drastically increase the cost of the integration step, a significant worry where multiple fields are to be calculated. Similarly, too small values for T do not give particles enough time to separate, producing poorly defined ridges. Choosing T becomes even more complicated when grid spacing is factored in. Calculating the gradient of the flow map we accomplish with finite differencing, an approximation that improves as the grid spacing is decreased, and the blob of points around $\mathbf{x}$ moves closer together. But as grid spacing becomes truly infinitesimal then it takes longer and

longer for two points to separate sufficiently, even those on or close to the LCS. It is entirely possible to define a grid so dense that the time required to resolve the LCS becomes impractical. With such dense grids even seemingly large choices of T can give low FTLE values for the LCS. Some coarseness to the grid allows points to straddle the ridge, and therefore separate much faster. Of course the steeper the slope of the LCS, the better it will resolve for even extremely fine grids, as two points on a steep slope take less time to separate than on a shallow one.

Both grid spacing and choice of T can often best be determined through simply testing different values. Computing the field first for a 'rough' grid spacing, then again with a double-accuracy grid, gives an indication as to how much further the grid needs be improved. Especially where initially using a fine grid will take a long period of time to produce any image, such an approach can save much potential frustration. Different values of T, on the other hand, will not merely *refine* the image (as with grid spacing), but will actually change the LCS detected. For a non-autonomous system, the LCS itself is advected by the flow, so may move about the field. The degree to which this occurs is entirely system dependent; there may be very little movement such that the LCS is virtually still, or there may be very great movement, such that the LCS snakes across the FTLE field. If we are in the situation where the LCS moves alot, then we expect to see more of this movement as T increases. If it takes 10 time units for the LCS to move to a given region of the field, then obviously we require $T > 10$ for the FTLE field to detect the LCS in that region. The FTLE field produced is like a long-exposure photograph, which captures in a single shot *all* movement occuring over the exposure time (i.e. T). Car headlights, for instance, stretch to form long light trails in this manner. A better method for finding the movement of the LCS is to compute FTLE fields for a sequence of t values, all using a single T, which is not too large. If the LCS is moving we still will not be seeing the exact LCS, as it is still like the long-exposure photograph, but this is not necessarily a problem. The movement of the LCS will be shown as a coherent line travelling around the field, rather than the stretching that would occur if we merely adjusted T.

While we may not know the exact length of the 'true' LCS, we can still learn important information about the system from the FTLE field. Low FTLE values indicate relatively stationary particles, such that where an LCS extends between two low FTLE regions, particles are being advected away from the LCS into these areas. Even if the LCS then moves on, these particles will not flow back very rapidly - if they did then this would indicate high FTLE values in these regions, which is not the case. Yet this will still produce very complicated mixing patterns, dependent on the complexity of the LCSs movements through the field. More useful, though, is an LCS that moves in relatively *fixed* fashion, staying between two regions throughout the course of its movement. We already know that given an appropriately formed LCS, there is minimal flow across the structure, meaning that we can rely on the ridgeline to effectively separate areas of the field. This produces the distinct mixing regions we originally developed these methods to locate. How the LCS is seen to move over the sequence of t values, then, is vastly important in classifying the stability of the system, and has important real world implications. Figure 6

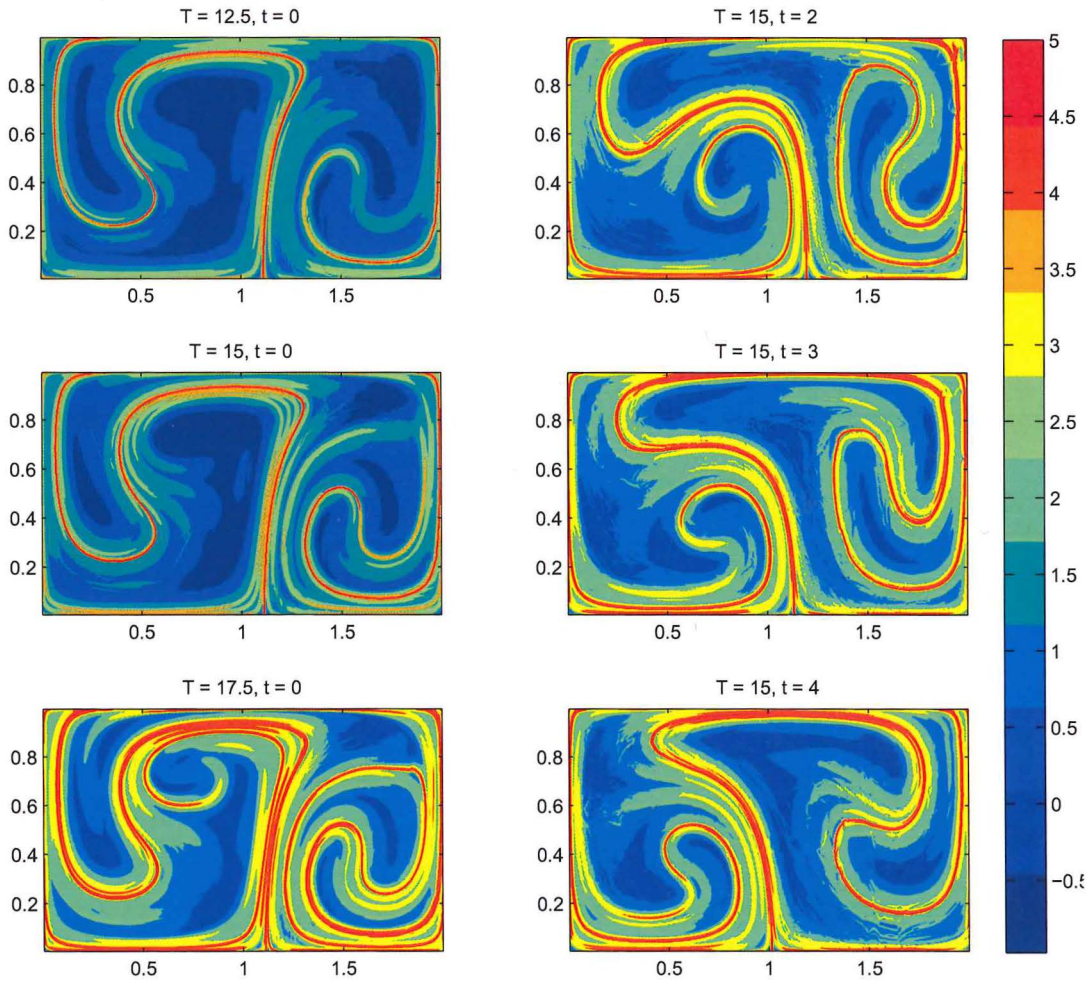

Figure 6: FTLE fields for various t and T values, 512x256 points

displays the changes that occur for the FTLE plot as t is fixed and T varied, or T fixed and T varied; actual t and T values are given for each plot.

To extract the LCS from the FTLE field we may proceed in one of two ways. The first method is to compute the Hessian at each point, as well as the gradient field. Along the LCS the eigenvector corresponding to the minimum (i.e. most negative) eigenvalue of the Hessian gives the $\hat{\mathbf{n}}$ direction, and the gradient field gives the $\hat{\mathbf{t}}$ direction. The inner product of the two should then give the level set $L = 0$. However, while the Hessian is easily calculated, the gradient field is not, at least not in a numerically stable way. This is because the gradient increases very rapidly where slightly off the ridge, as the curvature is maximized in the vicinity of the ridgeline. Instead we use a second, more convenient method. Since the ridgelines are so much higher than the rest of the FTLE field, we can simply look at the highest point in the field, and get rid of all points below a certain threshold. As long as the ridgeline doesn't vary too much and the threshold is chosen sufficiently high up the ridge (and consequently above the rest of the field), such a method will pick out only the top portion of the ridgeline. This second method finds the very problem of the first method an advantage, that of ridge sharpness. Here it means that very little of the ridge other than the very top remains when we discard 'low' points, and thus what we are left with is a good approximation to the ridge.

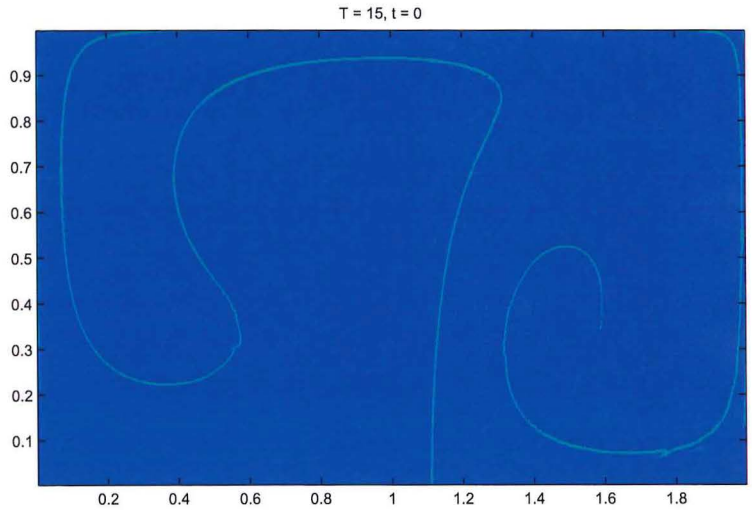

Figure 7: LCS as extracted from FTLE field by dismissing 'low' points

6. Applications

The most obvious application of LCS theory is for fluid flows, which are naturally phrased in terms of mixing regions and trajectories. Shadden, Lekien and Marsden (2005) undertook a study using Very High Frequency (VHF) radar to collect ocean velocity data, off the coast of

Florida. Computing FTLE fields found an LCS that varied within a narrow band extending south-east of the shore, such that the region off the coast was divided into two separate regions. In the context of an ocean outflow pipe, this meant that if released north-east of the LCS, pollutants were rapidly carried out to sea, in a matter of hours. In contrast, those released south-west of the structure were recirculated near shore, before slowly drifting outwards. Importantly this information was not obvious from direct inspection of the velocity fields. Only when computation of the FTLE fields were carried out did such behaviour become apparent. Interestingly Shadden also compared the flux rate with the average particle velocity for the field, and found that particles crossed the LCS at maximum rate of less than 0.05% of that of the average.

A less obvious application is one by Aldridge, Haller and Sorger (2006) in which he looks at transient signalling involved in apoptosis (programmed cell death). Previous studies have looked at apoptosis in terms of life-death steady states, but cell fates are decided long before these states are ever reached. And especially where some 8 different factors contribute to cell-fate, steady state models can be incredibly difficult to analyze. The LCS approach simplifies analysis hugely, by taking 3 dimensional subsets and looking for separatrices (i.e. LCSs). These quantitatively identify points at which a continuous change in species concentration leads to a dramatic, discontinuous change in response. Biologically we expect the apoptosis regulatory network to have a separatrix, as a cell's response is survival or death - it is never graded. Here a separatrix was found in the (activated) *caspase-8*:*XIAP* (X-linked inhibitor of apoptosis) plane, where *caspase-8* is an initiator and *XIAP* is an inhibitor. It was also not found to move noticeably with time, which seems sensible in a biological context. Note that the FTLE field reinforced the basic assumption of non-graded responses, as if these were possible then one would expect FTLE values to be more uniform across the field, which was not the case. Also note that in this paper FTLEs are referred to as *Direct* Lyapunov Exponents (DLEs), and are calculated without the $1/|T|$ scaling factor. Yet even without the additional computation of the scaling factor, each FTLE plot in this study took more than *60 hours* to compute.

A variety of other uses have been explored in the still-young field of LCS analysis. Shadden and Eldredge (2006) looked at separation profiles over an airfoil, finding an LCS that divides 'free-stream flow' from the 'dead-water zone' (i.e. zone of recirculation). This separation profile behaves like an unstable manifold, attracting and ejecting particles near the separation point, and was found using a *negative* integration time. Shadden, Marsden and Dabiri (2006), on the other hand, looked at fluid flows in the context of a swimming jellyfish. Here the creature actually controls the movement of LCSs, in order to entrain fluid (and nutrients) within the subumbrellar region of the creature (an open cavity with a similar function to a stomach). Shadden and Taylor (2008) have also applied LCS theory to cardiovascular flow studies. Using MRI data for the computation of LCSs can detect zones of recirculation, and, more importantly, whether these remain stationary. If they do, then this can lead to the formation of blood clots and plaque build-up, also known as hardening of the arteries. These are just a few examples

of the current uses of LCS theory, which hopefully demonstrate the real world nature of these structures. It is crucial to understand that FTLE fields are not merely abstract mathematical constructions, but are a quantitative description of the behaviour of systems over time. It is from these descriptive fields that we are able to locate special dividing ridges, which are our LCSs.

Conclusion

The use of FTLEs enables the understanding of a great deal of otherwise complicated system behaviour by simple visual inspection. Such a method is of obvious use where solving analytically is not feasible. This is generally the case with non-autonomous systems, as a Eulerian approach does not suit time-varying systems. Effective use of FTLEs requires considerable understanding of what a Lagrangian coherent structure actually is, and it is this that this paper sought to explain. Here an LCS was taken to be a second-derivative ridge of the FTLE field, but this is not the only possible definition; the second-derivative ridge was shown to be a *subset* of the more-general curvature ridge definition. Mainly it was due to computational ease that the second-derivative ridge was favoured, as issues of computational efficiency are of major concern in the numerical implementation of LCS theory. In fact we found that the name LCS is something of a misnomer, as ridgelines were shown to be only approximately Lagrangian. How Lagrangian depends on the field itself, the flux directly related to integration time, sharpness of the ridge, how greatly the ridges varies along its length, and whether the ridge rotates at a similar speed to the velocity field.

This study of LCS theory has been restricted to flows occuring in two-dimensional spaces, yet this was for the sake of simplicity only. All the ideas developed here may be extended into higher-dimensional space. The apoptosis study is one such example, taking three-dimensional subsets of an eight-dimensional space, in search of separatrices (LCSs). If anything, higher-dimensional study makes LCS theory *more* appropriate, as the complexity of traditional approaches rapidly increases. And with thanks to developments in both computers and numerical methods, computation of FTLE fields is becoming even easier, within the means of the average home PC, albeit with some time cost. LCS methods apply to a huge variety of systems, especially since many if not most real world systems exhibit time dependence. Especially in the context of the life sciences, a broadening area of mathematical research, LCS theory looks set to become one of the major tools of dynamical system analysis.

References

Aldridge, B.B., Haller, G., Sorger, P.K., Lauffenburger, D.A. (2006) Direct Lyapunov exponent analysis enables parametric study of transient signalling governing cell behaviour

Systems Biology, IEE Proceedings, Vol. 153, No. 6 Pg. 425 - 432

Barreira, L., Pesin, Y. (2002) Lyapunov Exponents and Smooth Ergodic Theory *University Lecture Series, vol. 23, American Mathematical Society, Providence, RI*

Doerner, R., Hubinger, B., Martienssen, W., Grossmann, A., Thomae, S. (1999) Stable manifolds and predictability of dynamical systems *Chaos, Solitons and Fractals 10 (11)* Pg. 17591782

Haller, G., Poje, A.C. (2000) Finite-time transport in aperiodic flows *Physica D 119* Pg. 352380

Haller, G. (2000) Lagrangian coherent structures and mixing in two-dimensional turbulence *Chaos 10 (1)* Pg. 99108

Haller, G., Yuan, G. (2000) Lagrangian coherent structures and mixing in two-dimensional turbulence *Physica D 147* Pg. 352370

Haller, G. (2001) Distinguished material surfaces and coherent structures in 3d fluid flows *Physica D 149* Pg. 248277

Haller, G. (2002) Lagrangian coherent structures from approximate velocity data *Physics of Fluids, Volume 14, Issue 6* Pg. 18511861

Liapunov, A.M. (1966) Stability of Motion *Academic Press, New York*

ONeill, B. (1997) Elementary Differential Geometry *2nd ed., Academic Press, San Diego*

Oseledec, V.I. (1968) A multiplicative ergodic theorem: Ljapunov characteristic numbers for dynamical systems *Trans. Moscow Math. Soc. 19* Pg. 197231

Ottino, J.M. (1989) The Kinematics of Mixing: Stretching, Chaos, and Transport *Cambridge University Press, Cambridge*

Pierrehumbert, R.T., Yang, H. (1993) Global chaotic mixing on isentropic surfaces *J. Atmospheric Sci. 50* Pg. 24622480

Shadden, S.C., Dabiri, J.O., Marsden, J.E. (2006) Lagrangian analysis of fluid transport in empirical vortex ring flows *Physics of Fluids 18 (4): 047105*

Shadden, S.C., Eldredge, J. (2006) A dynamical systems approach to unsteady systems *California Institute of Technology Pasadena, California*

Shadden, S.C., Lekien, F., Marsden, J.E. (2005) Definition and properties of Lagrangian coherent structures from finite-time Lyapunov exponents in two-dimensional aperiodic flows *Physica D 212(3-4)* Pg. 271-304

Shadden, S.C., Taylor, C.A. (2008) Characterization of Coherent Structures in the Cardiovascular System *Annals of Biomedical Engineering 36(7)* Pg. 1152-1162

Truesdell, C.A. (1954) The Kinematics of Vorticity *Indiana University Press, Bloomington*

Appendix 1 - Analytical model of a double-gyre flow

Here we take time to explain the periodically varying double-gyre model used as an example throughout this paper. Such flow is described by the stream-function

$$\psi(x,y,t) = A\sin(\pi f(x,t))\sin(\pi y) \tag{1}$$

where

$$f(x,t) = a(t)x^2 + b(t)x \tag{2}$$

$$a(t) = \epsilon\sin(\omega t) \tag{3}$$

$$b(t) = 1 - 2\epsilon\sin(\omega t) \tag{4}$$

over the domain [0,2] x [0,1]. This model should be seen as a simplification of a double-gyre pattern that occurs in geophysical flows, not as the approximate solution to a real flow (Shadden et al. (2005)). The forms of the parameters a and b are chosen to produce a simple time-dependent flow with fixed boundaries.

As $\psi(x,y,t)$ is a stream function, the flow velocities are defined as follows:

$$u = -\frac{\partial\psi}{\partial y} = -\pi A\sin(\pi f(x,t))\cos(\pi y) \tag{5}$$

$$v = \frac{\partial\psi}{\partial x} = \pi A\cos(\pi f(x,t))\sin(\pi y)\frac{df}{dx} \tag{6}$$

Where u and v are the velocities in the x and y coordinate directions, respectively. This formulation of the stream function satisfies the two dimensional continuity equation:

$$\frac{du}{dx} + \frac{dv}{dy} = 0 \tag{7}$$

For $\epsilon \neq 0$ the flow is time-dependent, the two gyres conversely expanding and contracting periodically in the x-direction, such that the rectangle enclosing the gyres remains invariant. In equation (1), A determines the magnitude of the velocity vectors, $\omega/2\pi$ is the frequency of the oscillation, and ϵ is approximately how far the line separating the gyres moves to the left or right. We can show this by considering the motion of the separation point $\widetilde{x}$ on the x axis about the point (1,0). First, however, we need to know where $\widetilde{x}$ is located; since $\widetilde{x}$ is on the line

that separates the gyres, we look for where there is no horizontal motion, i.e. $u = 0$. This will be either where $f(x) = 0$, or $f(x) = 1$. From the quadratic equation, we can therefore find the separation point $\widetilde{x}$ on the x axis, as follows (note that not all the quadratic equation solutions are shown here, as these pick out solutions not of interest, such as the lines $x = 0$ and $x = 2$).

$$\begin{aligned} f(x) = 1 &= \epsilon \sin(\omega t)x^2 + (1 - 2\epsilon \sin(\omega t))x \\ x &= \frac{-(1-2\epsilon \sin(\omega t)) + \sqrt{(1-2\epsilon \sin(\omega t))^2 + 4\epsilon \sin(\omega t)}}{2\epsilon \sin(\omega t)} \\ x &= \frac{2\epsilon \sin(\omega t) - 1 + \sqrt{1 + 4\epsilon^2 \sin^2(\omega t)}}{2\epsilon \sin(\omega t)} \end{aligned} \tag{8}$$

Now we look at the distance between $\widetilde{x}$ and the point (1,0),

$$\begin{aligned} \widetilde{x} - 1 &= \frac{2\epsilon \sin(\omega t) - 1 + \sqrt{1 + 4\epsilon^2 \sin^2(\omega t)}}{2\epsilon \sin(\omega t)} - 1 \\ &= \frac{\sqrt{1 + 4\epsilon^2 \sin^2(\omega t)} - 1}{2\epsilon \sin(\omega t)} \\ &\approx \frac{1 + 2\epsilon^2 \sin^2(\omega t) - 1}{2\epsilon \sin(\omega t)}, \qquad \text{for small } \epsilon \\ &= \epsilon \sin(\omega t) \end{aligned} \tag{9}$$

Thus we have shown that ϵ is approximately how far the line separating the gyres moves to the left or right, where ϵ is small. The figure below displays this movement, showing the separatrix at its furtherest position to the right, for $\epsilon = 0.25$

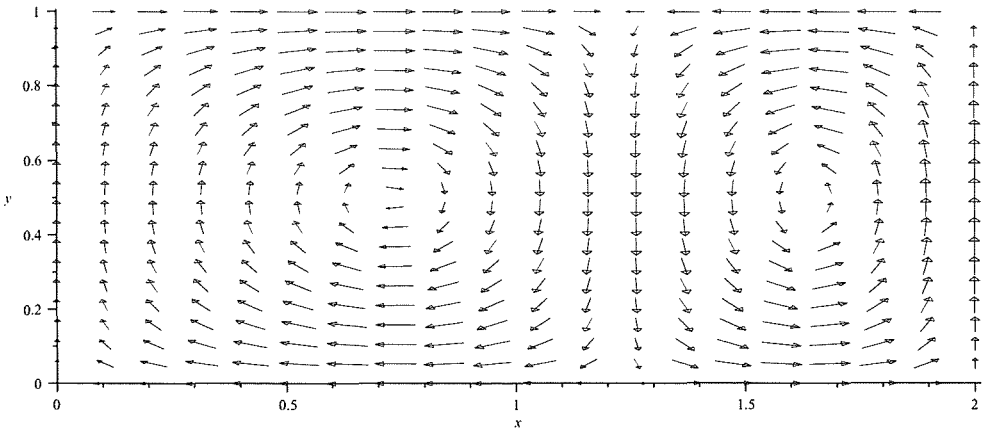

Figure 1: Velocity field for double gyre at $t = 0.25$, with $A = 0.1$, $\omega = 2\pi$, and $\epsilon = 0.25$

Appendix 2 - Proving $\mathcal{L}\hat{\mathbf{n}} = 0$

Our aim here will be to show that $\mathcal{L}\hat{\mathbf{n}} = 0$, where $\mathcal{L}$ is the Hessian of L. Such a proof must be done in 4 distinct stages, only 3 of which we will fully explain here, due to space restrictions and the fact that it is already well-explained by Shadden et al. (2005). These stages are as follows: 1) to show that $\mathbf{c}(s)$ is C^2 in space, 2) show that each $x \in U_t$ has a unique $\mathbf{x}_q$ on the LCS, where U_t is an open set containing the LCS, 3) show that ∇L is C^1 over U_t, and 4) that $\mathcal{L}\hat{\mathbf{n}} = 0$ everywhere in U_t. It is stage 2 that we shall not prove here.

Stage 1

We already know that $\sigma(\mathbf{x})$ is C^2 in space and C^1 in time. Therefore $\nabla\sigma(\mathbf{c}(s))$ is C^1 in space. By **SR2**, $\mathbf{c}'(s)$ is necessarily parallel to $\nabla\sigma(\mathbf{c}(s))$, and so is also C^1 in space. Thus, $\mathbf{c}(s)$ is C^2 in space.

Stage 2 - not shown here. However it should be said that proving that each $x \in U_t$ has a unique $\mathbf{x}_q$ relies on the above continuity of $\mathbf{c}(s)$. This is because C^2 continuity means that the curvature of $\mathbf{c}(s)$ remains finite. We are then able to give a proof by contradiction, by assuming that for some $x \in U_t$, $\mathbf{x}_q$ is non-unique.

Stage 3

Since we have $L(\mathbf{x}, t) = \pm \parallel \mathbf{x} - \mathbf{x}_q \parallel$, we can form the directional derivative of L as,

$$\nabla L = \frac{\pm 1}{\parallel \mathbf{x} - \mathbf{x}_q \parallel} \left\langle I - \frac{d\mathbf{x}_q}{d\mathbf{x}}, \mathbf{x} - \mathbf{x}_q \right\rangle \tag{1}$$

which should be sufficiently clear, since $\nabla L = 0$ along the trajectory.

But we already know that $\left\langle \frac{d\mathbf{x}_q}{d\mathbf{x}}, \mathbf{x} - \mathbf{x}_q \right\rangle = 0$, as the closest point on the LCS does not change with variation in the direction normal to the curve. Therefore we can write

$$\nabla L = \frac{\mathbf{x} - \mathbf{x}_q}{\pm \parallel \mathbf{x} - \mathbf{x}_q \parallel} = \frac{\mathbf{x} - \mathbf{x}_q}{L} = \hat{\mathbf{n}}(\mathbf{x}, t) \tag{2}$$

where we have used the fact that $\mathbf{x}_q$ is the point on the LCS closest to $\mathbf{x}$. Hence $\hat{\mathbf{n}}(\mathbf{x}, t)$ must be parallel to $\mathbf{x} - \mathbf{x}_q$.

By **Stage 2**, we know that there is a unique $\mathbf{x}_q$ for each $x \in U_t$. As a result, $\hat{\mathbf{n}}(\mathbf{x}, t)$ is a well-defined function of $\mathbf{x}$. Furthermore, by **Stage 1**, $\mathbf{c}'(s)$ is C^1 in space (and $\neq 0$), and so therefore is ∇L, as

$$\nabla L = \widehat{\mathbf{n}}(\mathbf{x}, t) = \widehat{\mathbf{k}} \text{ x } \widehat{\mathbf{t}} = \widehat{\mathbf{k}} \text{ x } \mathbf{c}' / \parallel \mathbf{c}' \parallel \tag{3}$$

where $\widehat{\mathbf{k}}$ is the unit basis vector pointing 'up' from the domain D. Note that this also implies that L is C^2 in space.

Stage 4

By the above, we know that ∇L exists and is differentiable. In particular, $\parallel \nabla L \parallel = 1$, as $\nabla L = \widehat{\mathbf{n}}(\mathbf{x}, t)$, so that we have

$$0 = \nabla(\parallel \nabla L \parallel^2) = 2\mathcal{L}\nabla L = 2\mathcal{L}\widehat{\mathbf{n}} \tag{4}$$

Hence we have shown that $\mathcal{L}\widehat{\mathbf{n}} = 0$, as required.

```
function ftle_field
%Appendix 3: LCS Research Project, Matt Botur, 73230203
%FTLE Field, Double Gyre, Time Dependent
clear;clc;

%% Parameters (T,t, A etc.) to be defined here %%
%% Pre-allocate matrices according to gridsize %%

%%%% Numerical Computation of Points %%%%
for I = 1:n
    for J = 1:m
        [Time,CART] = ode45(@d_gyre_time_eq,[t t+T],[X1(I,J); Y1
(I,J)],options);
        p=length(CART);X2(I,J)=CART(p,1);Y2(I,J)=CART(p,2);
    end
end
%%%%%%%%%%%%%%%%%%%%%%%%%%%%%%%%%%%%%%%%%%%%

%%%% Computation of FTLEs %%%%
for I = 2:n-1
    for J = 2:m-1
        D = [(X2(I,J+1)-X2(I,J-1))/(X1(I,J+1)-X1(I,J-1)) (X2(I+1,J)-X2
(I-1,J))/(Y1(I-1,J)-Y1(I+1,J));
            (Y2(I,J-1)-Y2(I,J+1))/(X1(I,J+1)-X1(I,J-1)) (Y2(I-1,J)-Y2(I+
1,J))/(Y1(I-1,J)-Y1(I+1,J))];
        Z(I,J) = log(norm(D,2));
    end
end
%%%%%%%%%%%%%%%%%%%%%%%%%%%%%%%

%%%% Plotting Code: FTLE Field %%%%
figure(1)
surfc(x(2:m-1),y(2:n-1),Z(2:n-1,2:m-1))
colormap(jet(11));colorbar;title('FTLE Surface Plot, T = 15, t = 0');
%%%%%%%%%%%%%%%%%%%%%%%%%%%%%%%%%%

%%%% Selects LCS by dismissing low points %%%%
a=max(max(Z));b=min(min(Z));
L(find( Z > (a-((a-b)*0.2)))) = 1;
%%%%%%%%%%%%%%%%%%%%%%%%%%%%%%%%%%%%%%%%%%%%%%%%%%%%

%%%% Plotting Code: Extracted LCS %%%%
figure(2)
contourf(x(2:m-1),y(2:n-1),L(2:n-1,2:m-1), 'Edgecolor','none');
colormap(jet(2));title('LCS Plot, T = 15, t = 0');
%%%%%%%%%%%%%%%%%%%%%%%%%%%%%%%%%%%%

    function dcart = d_gyre_time_eq(t,cart)
        dcart = zeros(2,1);
        a = epsilon*sin(omega*t); b = 1 - 2*a;
        f = a*(cart(1)^2) + b*cart(1);df = 2*a*cart(1) + b;
        dcart(1) = -pi*A*sin(pi*f)*cos(pi*cart(2));
        dcart(2) = pi*A*cos(pi*f)*sin(pi*cart(2))*df;
    end
end
```